AD-A049 636 DAVID W TAYLOR NAVAL SHIP RESEARCH AND DEVELOPMENT CE--ETC F/G 1/3
ANALYSIS OF EMPIRICALLY DETERMINED AERODYNAMIC AND RAM COEFFICI--ETC(U)
OCT 77 D G ROUSSEAU

UNCLASSIFIED DTNSRDC/ASED-396 NL

1 OF 1
AD
A049 636

END
DATE
FILMED
3-78
DDC

1 OF 1

AD
A049 636

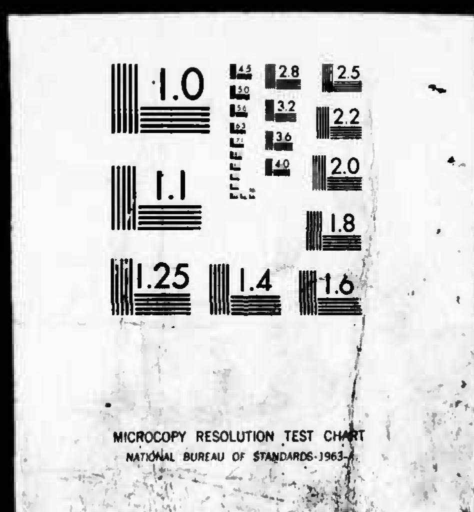

12

B.S.

DEPARTMENT OF THE NAVY
DTNSRDC

6

ANALYSIS OF EMPERICALLY DETERMINED AERODYNAMIC AND RAM COEFFICIENTS FOR A POWER-AUGMENTED-RAM WING-IN-GROUND EFFECT.

by

10 David G. Rousseau

9 Final rept. Jun-Oct 77,

Approved for Public Release: Distribution Unlimited

AVIATION AND SURFACE EFFECTS DEPARTMENT

16 SSH15, WF41421

17 SSH15002, WF41421160

14 DTNSRDC/ASED-396

11 Oct [redacted] 77

12 22p.

DAVID W. TAYLOR NAVAL SHIP RESEARCH AND DEVELOPMENT CENTER

BETHESDA MARYLAND 20084

UNCLASSIFIED

SECURITY CLASSIFICATION OF THIS PAGE (When Data Entered)

REPORT DOCUMENTATION PAGE

READ INSTRUCTIONS BEFORE COMPLETING FORM

1. REPORT NUMBER
DTNSRDC ASED-396

2. GOVT ACCESSION NO.

3. RECIPIENT'S CATALOG NUMBER

4. TITLE (and Subtitle)
ANALYSIS OF EMPIRICALLY DETERMINED AERODYNAMIC AND RAM COEFFICIENTS FOR A POWER-AUGMENTED-RAM WING-IN-GROUND EFFECT

5. TYPE OF REPORT & PERIOD COVERED
Final
Jun-Oct 1977

6. PERFORMING ORG. REPORT NUMBER

7. AUTHOR(s)
David G. Rousseau

8. CONTRACT OR GRANT NUMBER(s)

9. PERFORMING ORGANIZATION NAME AND ADDRESS
Aviation and Surface Effects Department
David W. Taylor Naval Ship R&D Center
Bethesda, MD 20084

10. PROGRAM ELEMENT, PROJECT, TASK AREA & WORK UNIT NUMBERS
See reverse side

11. CONTROLLING OFFICE NAME AND ADDRESS
Naval Air Systems Command
Code AIR-032D
Washington, D.C. 20361

12. REPORT DATE
October 1977

13. NUMBER OF PAGES
20

14. MONITORING AGENCY NAME & ADDRESS (if different from Controlling Office)

15. SECURITY CLASS. (of this report)
Unclassified

15a. DECLASSIFICATION/DOWNGRADING SCHEDULE

16. DISTRIBUTION STATEMENT (of this Report)
Approved for Public Release: Distribution Unlimited

17. DISTRIBUTION STATEMENT (of the abstract entered in Block 20, if different from Report)

18. SUPPLEMENTARY NOTES

19. KEY WORDS (Continue on reverse side if necessary and identify by block number)
Power-Augmented-Ram Wing-In-Ground-Effect (PAR-WIG) Vechile
Data Analysis
Coefficients of Lift, Drag, and Pitching Moment

20. ABSTRACT (Continue on reverse side if necessary and identify by block number)

With the advent of a theory for power-augmented-ram wing-in-ground-effect vehicle performance, there is a need for detailed comparison with test data. This report presents a comparison of test data with theory, in particular, the determination of the effects of changes in vehicle geometry

(Continued on reverse side)

(Block 10)

Program Element 62241N
Project F41.421
Task WF41.421.1301
Work Unit 1600-077

Block 20 - continued)

and cruising height on flight performance. Good correlation between theory and experiment has been achieved for lift and pitching moment, and correlation with drag is promising for some geometries.

TABLE OF CONTENTS

LIST OF FIGURES

NOTATION

The majority of the analysis effort presented in this report deals with dimensionless coefficients and ratios. The dimensional parameters used are presented in the International System (SI) of units.

A_f	Area of ram channel entrance, m^2
A_{j_i}	Installed propulsor disk area, m^2
A_s	Area of sidewall or endplate gap, m^2
A_{TE}	Aera of trailing edge gap, m^2
A_w	Submerged or emersed area of endplate, m^2
C_D	Coefficient of aerodynamic drag from numerical analysis
C_{DP}	Coefficient of profile drag from momentum model
C_{D_R}	Coefficient of ram drag from numerical analysis
C_L	Coefficient of aerodynamic lift from momentum model
C_ℓ	Coefficient of aerodynamic lift from numerical analysis
C_M	Coefficient of aerodynamic pitching moment about the 40-percent chord
C_{M_R}	Coefficient of ram pitching moment about the 40-percent chord
C_P	Coefficient of pressure or ram lift
C_ρ	Calculated coefficient of pressure
$\bar{c}$	Mean aerodynamic chord, m
D	Experimental drag value, N
D_c	Calculated drag, N
L	Experimental lift value, N
L_c	Calculated lift, N
M	Experimental pitching moment value about the 40-percent chord, N·m

M_c	Calculated pitching moment, N·m
S	Wing planform area, m^2
T	Thrust, N
T_g	Gross thrust as a function of velocity, N
V_j	Propulsor exhaust velocity, m/sec
V_∞	Free stream velocity, m/sec
W	Vehicle weight, N
ε_D	Least squares drag error
ε_ℓ	Least squares lift error
ε_M	Least squares moment error
ρ_a	Density of air, kg/m^3
ρ_w	Density of sea water, kg/m^3
θ_f	Propulsor inclination angle, deg

ABSTRACT

With the advent of a theory for power-augmented-ram wing-in-ground-effect vehicle performance, there is a need for detailed comparison with test data. This report presents a comparison of test data with theory, in particular, the determination of the effects of changes in vehicle geometry and cruising height on flight performance. Good correlation between theory and experiment has been achieved for lift and pitching moment, and correlation with drag is promising for some geometries.

ADMINISTRATIVE INFORMATION

This investigation was undertaken by the WIG Project Group (1612) of the Aviation and Surface Effects Department at the David W. Taylor Naval Ship Research and Development Center (DTNSRDC). The model design, construction and testing was sponsored by the Advanced Naval Vehicle Concept Evaluation (ANVCE) Project Office (NOP-96V) of the Program Planning Office (Navy) and was funded under Task Area SSH15002, Work Unit 1[illegible]-009. This investigation was sponsored by the Naval Air Systems Command (NAIR-320D) and was funded under Task Area WF 41-421, Work Unit 1600-077.

INTRODUCTION

A continuing effort to analyze and compare experimental data with theory is vital to the understanding of the behavior of a new vehicle. The prevailing theory of Gallington (References 1 and 2) on power-augmented-ram (PAR) vehicle flight and the corresponding behavioral trends discerned by Rousseau (Reference 3) needed correlation with experimental

results. Thus, the accumulated test data* have been analyzed and compared with these theories. The effects of changes in certain parameters of vehicle geometry and flight operation are discussed, and good agreement with theory has been observed.

NUMERICAL ANALYSIS

The equations used in the analysis of the data are:

$$L_c = \rho_a V_j^2 A_{j_i} \sin \theta_f + C_\ell \frac{1}{2} \rho_a V_\infty^2 S + C_p \frac{1}{2} \rho_a V_j^2 S \qquad (1)$$

$$D_c = -T_g \cos \theta_f + \rho_a V_j V_\infty A_{j_i} + C_D \frac{1}{2} \rho_a V_\infty^2 S + C_{D_R} \frac{1}{2} \rho_a V_j^2 S \qquad (2)$$

and

$$M_c = C_M \frac{1}{2} \rho_a V_\infty^2 S\bar{c} + C_{M_R} \frac{1}{2} \rho_a V_j^2 S\bar{c} \qquad (3)$$

Nondimensionalizing by $\rho_a V_j^2 A_{j_i}$, and $\rho_a V_j^2 A_{j_i} \bar{c}$ for the moment equation, yields equations of the desired form that are not undefined at $V_\infty = 0$. After some manipulation these equations can then be expressed as

$$\varepsilon_\ell = \frac{L_c - L}{\rho_a V_j^2 A_{j_i}} \qquad (4)$$

---

* Reported informally by F. Krause ("Parametric Investigation of a Power-Augmented-Ram Wing over Water," DTNSRDC ASED TM-16-76-95, Oct 1976).

$$\varepsilon_D = \frac{D_c - D}{\rho_a V_j^2 A_{j_i}} \tag{5}$$

and

$$\varepsilon_M = \frac{M_c - M}{\rho_a V_j^2 A_{j_i} \bar{c}} \tag{6}$$

Equations (4), (5), and (6) now represent the differences, or errors, between the calculated and experimental values of lift, drag, and pitching moment, respectively. These differences are then used in the following least squares analysis equations

$$\frac{\partial}{\partial C_\ell} \Sigma\, \varepsilon_\ell^2 = 0 \qquad \frac{\partial}{\partial C_P} \Sigma\, \varepsilon_\ell^2 = 0 \tag{7 a,b}$$

$$\frac{\partial}{\partial C_D} \Sigma\, \varepsilon_D^2 = 0 \qquad \frac{\partial}{\partial C_{D_R}} \Sigma\, \varepsilon_D^2 = 0 \tag{8 a,b}$$

$$\frac{\partial}{\partial C_M} \Sigma\, \varepsilon_M^2 = 0 \qquad \frac{\partial}{\partial C_{M_R}} \Sigma\, \varepsilon_M^2 = 0 \tag{9 a,b}$$

where the summations are carried out over a given set of data acquired for a configuration of interest. Equations (7) through (9) will then allow the numerical determination of the six coefficients of interest such that the rms error is minimized over the data set considered.

This analysis was computerized so that the large amount of data* available could be easily handled.

COMPARISON TO MOMENTUM MODEL

The nondimensionalized equation for T-D from the filled duct solution of Reference 3 is

$$\frac{T-D}{\rho_a V_j^2 A_{j_i}} = -\frac{A_f}{A_{j_i}} + \frac{A_s}{A_{j_i}} \sqrt{C_p}\,(1-C_p)^{1/2} + \frac{A_{TE}}{A_{j_i}} - \frac{1}{2}\frac{\rho_W}{\rho_a}\left(\frac{V_\infty}{V_j}\right)^2 C_{f_w}\frac{A_w}{A_{j_i}}$$

$$-C_{DP}\frac{1}{2}\left(\frac{V_\infty}{V_j}\right)^2 \frac{S}{A_{j_i}} - \frac{V_\infty}{V_j} - C_{f_a}\frac{1}{2}(1-C_p)\frac{S}{A_{j_i}} - \frac{D_W}{\rho_a V_j^2 A_{j_i}}$$

and the nondimensionalized form of Equation (2) above is

$$\frac{-D_c}{\rho_a V_j^2 A_{j_i}} = \cos\theta_f - \frac{V_\infty}{V_j} - C_D\frac{1}{2}\left(\frac{V_\infty}{V_j}\right)^2\frac{S}{A_{j_i}} - C_{D_R}\frac{1}{2}\frac{S}{A_{j_i}}$$

See Figure 1 for a pictorial reference of the various coefficients. Equating these two expressions yields

$$\cos\theta_f - \frac{V_\infty}{V_j} - C_D\frac{1}{2}\left(\frac{V_\infty}{V_j}\right)^2\frac{S}{A_{j_i}} - C_{DR}\frac{1}{2}\frac{S}{A_{j_i}} = -\frac{A_f}{A_{j_i}} +$$

$$\frac{A_s}{A_{j_i}}\sqrt{C_p}\,(1-C_p)^{1/2} + \frac{A_{TE}}{A_{j_i}} - \frac{1}{2}\frac{\rho_W}{\rho_a}\left(\frac{V_\infty}{V_j}\right)^2 C_{f_W}\frac{A_W}{A_{j_i}}$$

$$-C_{DP}\frac{1}{2}\left(\frac{V_\infty}{V_j}\right)^2\frac{S}{A_{j_i}} - \frac{V_\infty}{V_j} - C_{f_a}\frac{1}{2}(1-C_p)\frac{S}{A_{j_i}} - \frac{D_W}{\rho_a V_j^2 A_{j_i}} \qquad (10)$$

* Ibid, p. 2

Separating into equations of like terms gives

$$\left[C_D\right]_{\text{Calculated}} = \left[C_{DP} + \frac{\rho_w}{\rho_a} C_{f_w} \frac{A_w}{S} + \frac{D_w}{\frac{1}{2}\rho_a V_\infty^2 S}\right]_{\substack{\text{Momentum}\\\text{Theory}}} \tag{11}$$

$$\left[C_{D_R} \frac{1}{2} \frac{S}{A_{j_i}} - \cos\theta_f\right]_{\text{Calculated}} = \left[-\frac{A_{TE}}{A_{j_i}} - \frac{A_S}{A_{j_i}} \sqrt{C_p}\,(1-C_p)^{\frac{1}{2}} + \frac{A_f}{A_{j_i}} + C_{f_a}(1-C_p)\frac{S}{2A_{j_i}}\right]_{\substack{\text{Momentum}\\\text{Theory}}} \tag{12}$$

At the high Froude numbers of interest, the wave drag (D_w) is inversely proportional to the velocity and becomes negligible. It is also evident that when the endplates are clear of the water, the immersed area of the endplates (A_w) will be zero, and that C_D varies linearly with A_w. Therefore, at high speeds with the endplates out of the water C_D will be nearly equal to the profile drag coefficient (C_{DP}).

The nondimensionalized equation for L = W from the filled duct solution of Reference 3 is

$$\frac{L}{\rho_a V_j^2 A_{j_i}} = \frac{1}{2} C_p \frac{S}{A_{j_i}} + \frac{1}{2} C_L \left(\frac{V_\infty}{V_j}\right)^2 \frac{S}{A_{j_i}}$$

The nondimensionalized form of Equation (1) is

$$\frac{L_c}{\rho_a V_j^2 A_{j_i}} = \sin\theta_f + C_\ell \frac{1}{2} \left(\frac{V_\infty}{V_j}\right)^2 \frac{S}{A_{j_i}} + C_p \frac{1}{2} \frac{S}{A_{j_i}}$$

Equating these two expressions yields

$$\left[\sin\theta_f + C_\ell \frac{1}{2}\left(\frac{V_\infty}{V_j}\right)^2 \frac{S}{A_{j_i}} + C_\rho \frac{1}{2}\frac{S}{A_{j_i}}\right]_{\text{Calculated}} = \left[\frac{1}{2} C_p \frac{S}{A_{j_i}} + \frac{1}{2} C_L \left(\frac{V_\infty}{V_j}\right)^2 \frac{S}{A_{j_i}}\right]_{\substack{\text{Momentum}\\\text{Theory}}} \tag{13}$$

Again, separating into equations of like terms gives

$$C_\ell = C_L \tag{14}$$

$$\left[\sin\theta_f + C_\rho \frac{1}{2}\frac{S}{A_{j_i}}\right]_{\text{Calculated}} = \left[C_p \frac{1}{2}\frac{S}{A_{j_i}}\right]_{\substack{\text{Momentum}\\\text{Theory}}} \tag{15}$$

Equation (14) shows that the lift coefficient arrived at by the numerical analysis represents the lift coefficient of the theory with no other effects included. The pressure coefficient of the theory, however, corresponds to the pressure coefficient of the numerical analysis plus a propulsor thrust component (Equation (15)). No comparison can be made with the equation of moment coefficients (Equation (6)) in that no such analysis was performed in the theoretical work of References 1, 2 and 3.

RESULTS AND DISCUSSION

Equation (14) indicates that both the numerical analysis C_ℓ and the C_L used in the momentum theory are equal. Figure 2a shows some indications of height effects on C_ℓ. The trend for most of the curves is that C_ℓ increases as height increases, but in all cases the C_ℓ appears to approach a value near 0.9 at a height of $h/\bar{c} = 0.21$. The apparently errant nature of some of the curves could correspond to some of the behavior observed by Pistolesi (Reference 4), although none of Pistolesi's cases involved power augmentation. The relationship between heave and C_p depicted in Figure 2b is more orderly, and the decrease in C_p as heave increases is predicted in References 1, 2, and 3. The effects of fan angle predicted in Equation (15) cannot be assessed in that all of the configurations represented are at $\theta_f = 20$ deg, which was found to be near optimum for this type of PAR wing-in-ground-effect (WIG) model. The fact that the slopes of the curves are all approximately the same is explained by the $\frac{1}{2}$ S/A_{j_i} terms in Equation (15), which are constant for all the geometries represented.

All of the points plotted in Figures 2a and 2b had rms errors of less than 10 percent. The two curves with $\delta_f = 20$ deg (Figures 3a and 3b) are less reliable because the majority of their points have rms errors greater than 10 percent. The sharp rise in C_D (Figure 3a) for very low heave values is clearly the result of endplate submergence. This agrees with Equation (11) in that for heaves of less than the endplate size (16.2%$\bar{c}$) the A_W/S term is no longer zero. Above that as the heave increases the C_D also increases, since the reduction of induced drag by ground effect is inversely related to cruising height. At heave values above $h/\bar{c}=0.21$, the C_D curves appear to converge at a value near 0.3, which would correspond

to the out-of-ground effect induced and profile drag coefficients of the vehicle.

A comparison of the $\delta_f = 20$ deg and $\delta_f = 40$ deg curves (for AR = 1.0) shows an increase in C_D as flap angle increases. This agrees with accepted aerodynamic theory. In Figure 3b the same change in δ_f results in an increase in C_{D_R}. This is supported by Equation (12) in that A_{TE} and δ_f are inversely related through geometry (Reference 3). However, C_{D_R} decreases with increasing heave, which again is evident in Equation (12) from the A_s/A_{j_i} term.

The effects of the terms of Equation (2) (after being non-dimensionalized) are presented in Figure 4. The constant-, first-, and second-order terms (dashed lines) are summed to yield the total caluclated value of the drag (solid curve). The comparison between this value and the experimental data (shown as mean points with ranges indicated) is fairly good.

The major discrepencies in the data seem to be indicative of hump drag effects. At the classical hump speed the depression of the water surface is greatest at the trailing edge of the vehicle's flap, resulting in a loss in ram pressure and a corresponding reduction in drag. This effect could be somewhat unrepresentative of actual vehicle behavior in that the model was not free in pitch. Pitch freedom would allow the vehicle to close the trailing edge gap by increasing its angle of attack, resulting in higher aerodynamic and ram drag as well as higher PAR cushion pressure. As the vehicle accelerates beyond hump speed, the point of maximum surface depression moves back. The effect of this shift is to decrease the relative surface depression at the trailing edge which enables the PAR-WIG to maintain its PAR pressure at lower angles of attack. The model, however, experienced the increase in PAR

cushion pressure and drag because it was not free to pitch. Another related effect would be the change in submergence of the aft portion of the endplates as the vehicle passes through hump. Endplate drag would be lower at hump speed in that the water surface is depressed; but, again, as the PAR-WIG accelerates the depression moves back and the endplates experience more wetted drag.

In Figures 5a and 5b all of the points plotted are for moments about the 40-percent chord and have very small rms errors, except for the lowest heave point of the AR = 0.5, δ_f = 20 deg curve which is somewhat less dependable. In both plots it is evident that the aerodynamic and ram moment coefficients both decrease as heave increases. The majority of the C_m data falls in the range from 0.2 to 0.25. Since these data are taken about the 40-percent chord, the effective center of pressure of the free-stream component is near the 25-percent chord. Most of the C_{MR} data fall in the range from 0.063 to 0.07 indicating that the effective center of ram pressure is very near the 40-percent chord where the data were taken. Also evident is an increase in aspect ratio yielding an increase in C_m, but the effects of aspect ratio on C_{MR} is unclear. In all of the cases studied the variations in C_{MR} are minor with about an 8.6-percent spread for the bulk of the data. The variations in the bulk of the C_m data are only about a 23-percent spread.

CONCLUSIONS

The analysis shows the lift coefficients are of acceptable magnitude at about 0.8, with the C_{PR} changing linearly with heave and varying from 0.6 to 0.3.

The coefficients of aerodynamic moment about the 40-percent chord range from nearly 0.2 to 0.25 and include the effects of lift from the fan shrouds. The ram moment coefficient, which includes the effects of the vertical component of fan thrust, stays nearly constant at about 0.066.

All rms errors for the lift and moment coefficients are 10-percent (or less), and most are below 5-percent.

The drag coefficient analysis provides a reasonable fit for a significant portion of the data. The coefficient of aerodynamic drag ranges from about 0.2 to 0.3 which includes profile and induced drag. The PAR cushion drag, which results from the change in the momentum of the propulsor efflux, and the propulsor intake ram drag constitute the C_{D_R}. The coefficient of ram drag varies from near 0.06 to about 0.02.

The drag equation needs to be modified to improve the result. The trends agree with the drag equation; however, rms errors of more than 20-percent occurred in half of the results. The effect of endplate submergence, for example, is very clear in the drag data and agrees with the drag equation. The modification of the wave drag term in the numerical analysis equation may improve the accuracy of the curve fit to some degree. This term was not modified initially because the PAR-WIG vehicle cruises at speeds well above hump speed, and transition through hump has never been a significant problem for this vehicle concept.

REFERENCES

1. Gallington, R. W., "Sudden Deceleration of a Free Jet at the Entrance to a Channel," DTNSRDC Report ASED 350 (Jan 1976).

2. Gallington, R. W. and H. R. Chaplin, "Theory of Power-Augmented-Ram Lift at Zero Forward Speed," DTNSRDC Report ASED 365 (Feb 1976).

3. Rousseau, D. G. and R. W. Gallington, "Performance Prediction Method for a Wing-In-Ground Effect Vehicle with Blowing Under the Wing," DTNSRDC Report ASED 379 (Mar 1977).

4. Pistolesi, E., "Ground Effect - Theory and Practice," NACA Report TM 828 (Jun 1937).

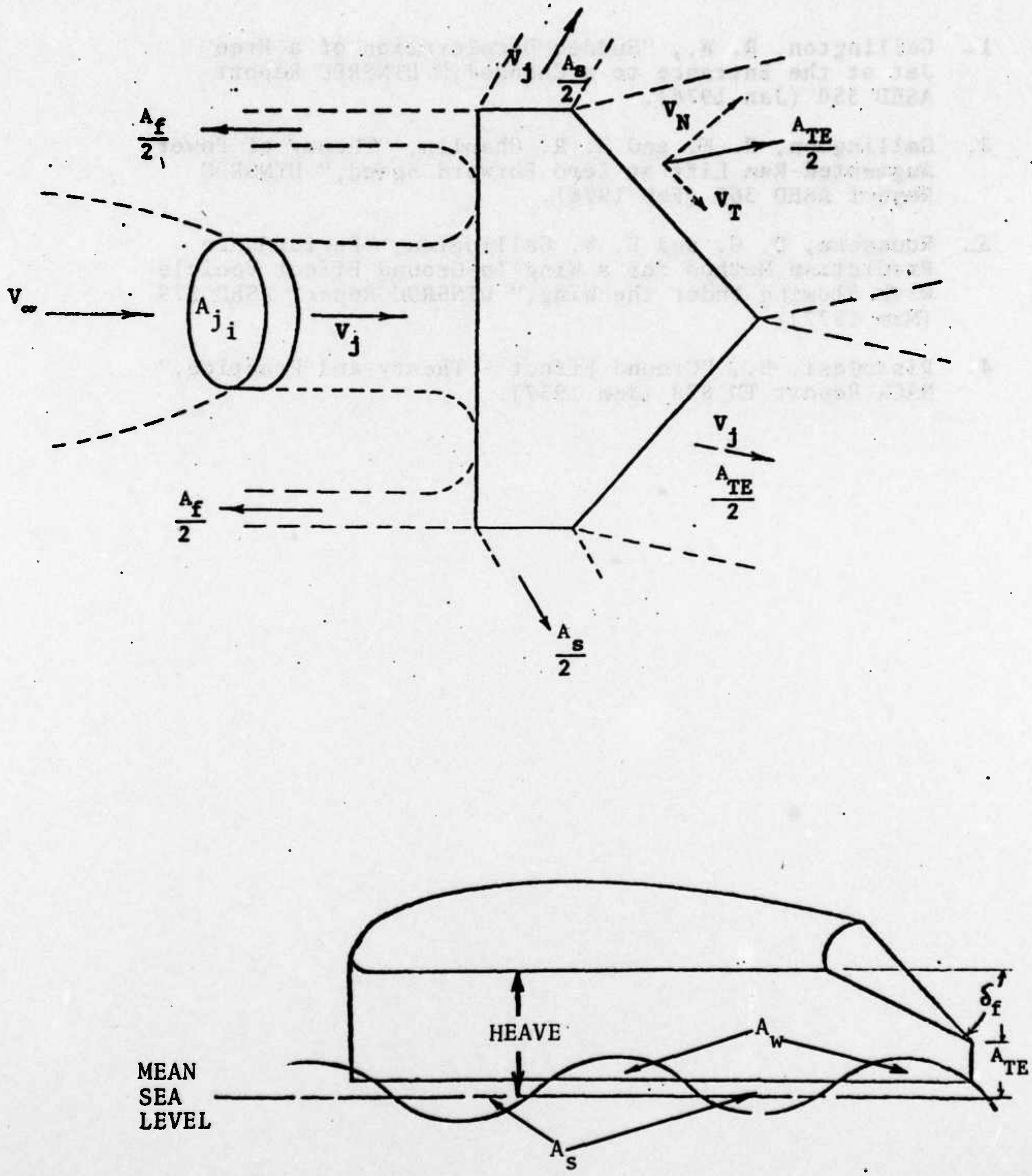

Figure 1 - Tapered PAR-WIG Schematic

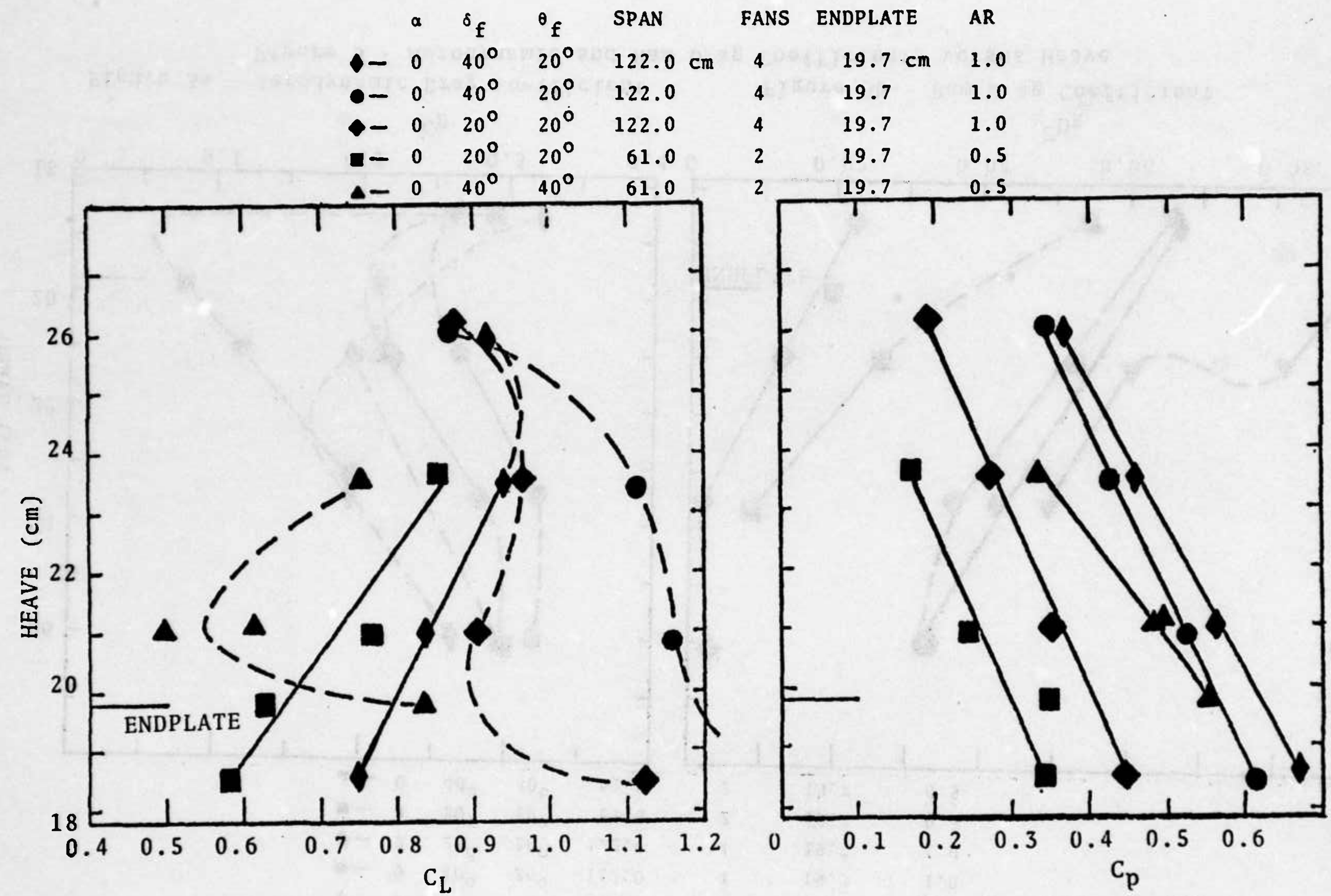

Figure 2a - Aerodynamic Lift Coefficient

Figure 2b - Ram Lift Coefficient

Figure 2 - Aerodynamic and Ram Lift Coefficients versus Heave

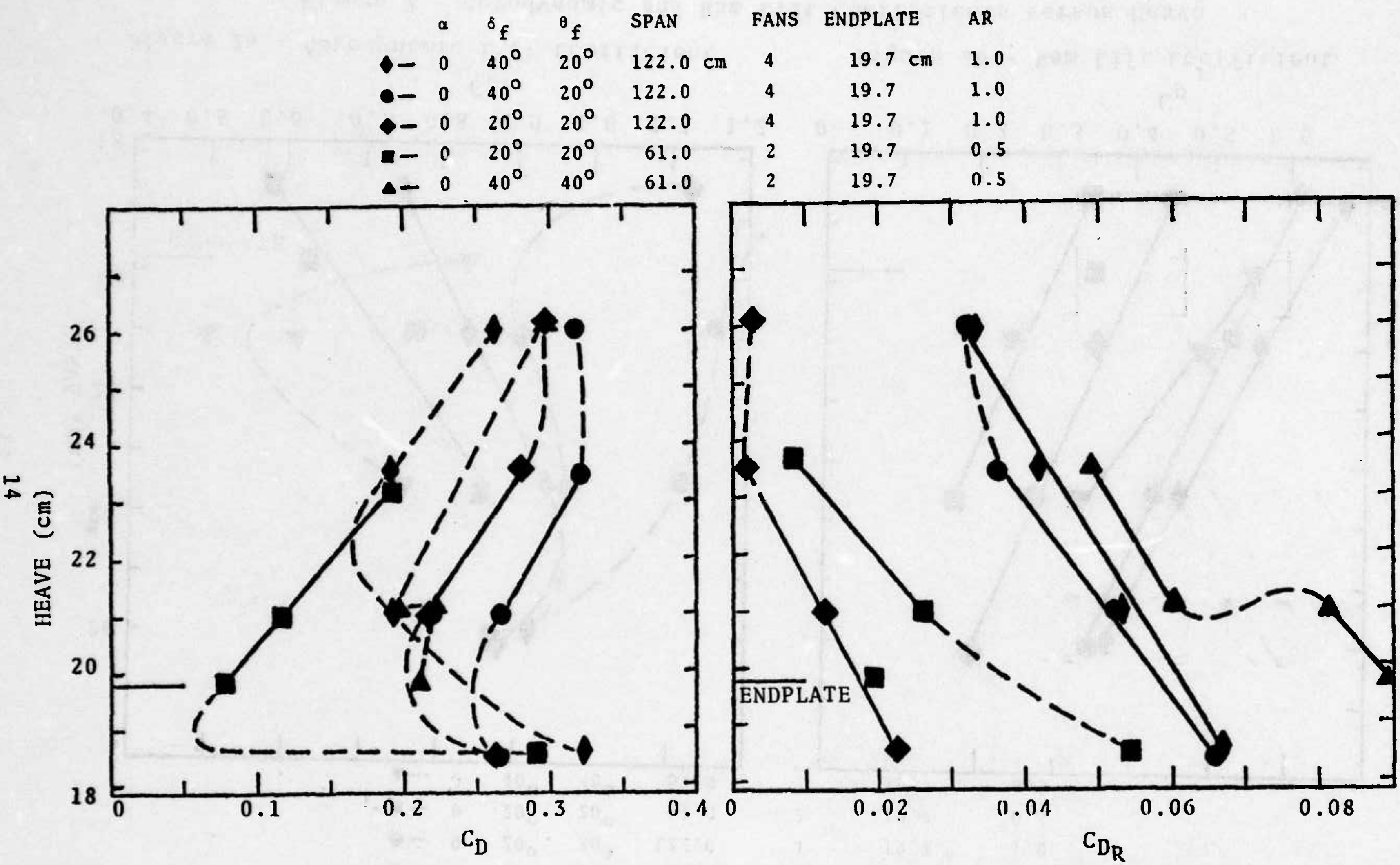

Figure 3a - Aerodynamic Drag Coefficient

Figure 3b - Ram Drag Coefficient

Figure 3 - Aerodynamic and Ram Drag Coefficients versus Heave

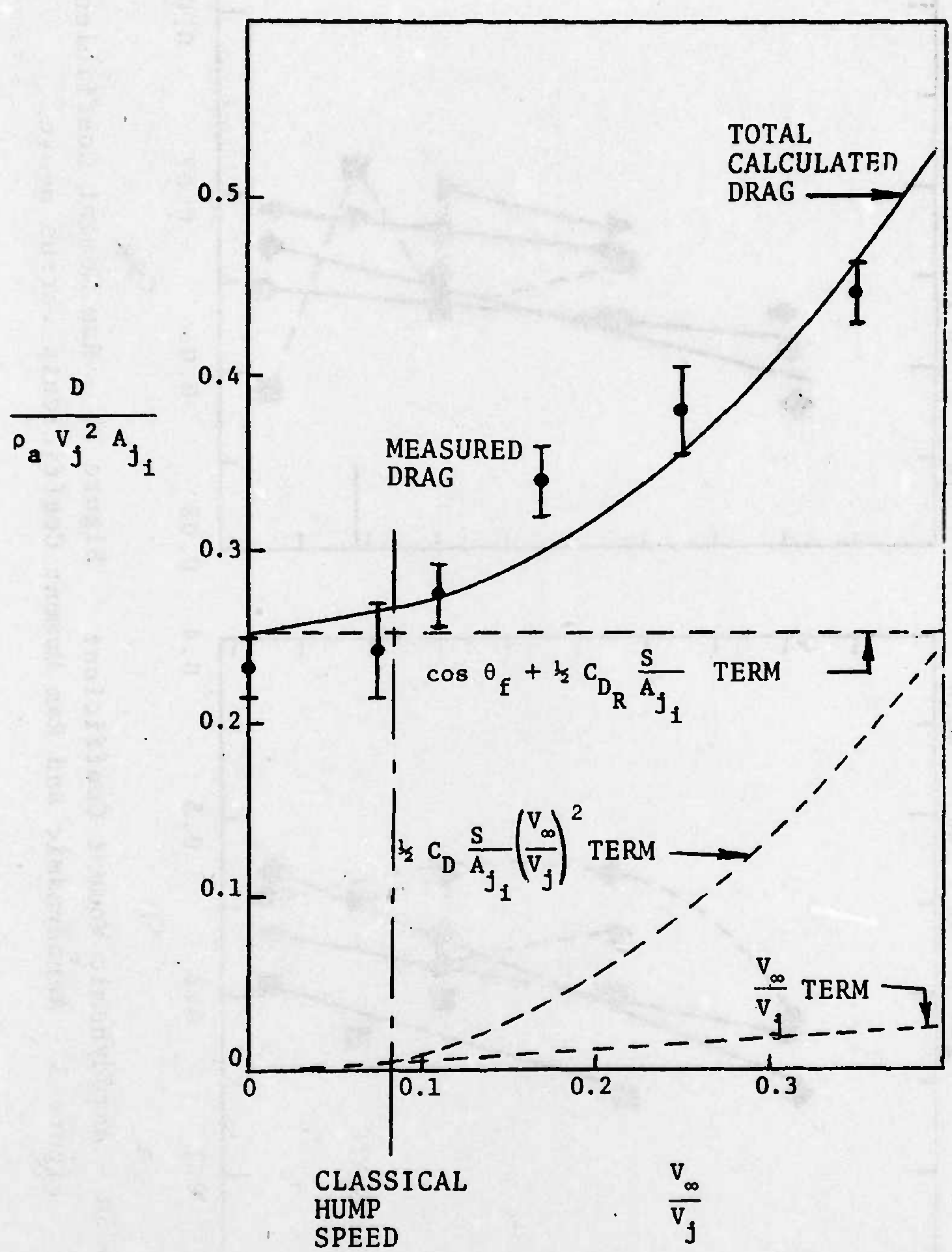

Figure 4 - Comparison of Measured and Calculated Drag

	α	δ_f	θ_f	SPAN	FANS	ENDPLATE	AR
◆—	0	40^o	20^o	122.0 cm	4	19.7 cm	1.0
●—	0	40^o	20^o	122.0	4	19.7	1.0
◆—	0	20^o	20^o	122.0	4	19.7	1.0
■—	0	20^o	20^o	61.0	2	19.7	0.5
▲—	0	40^o	40^o	61.0	2	19.7	0.5

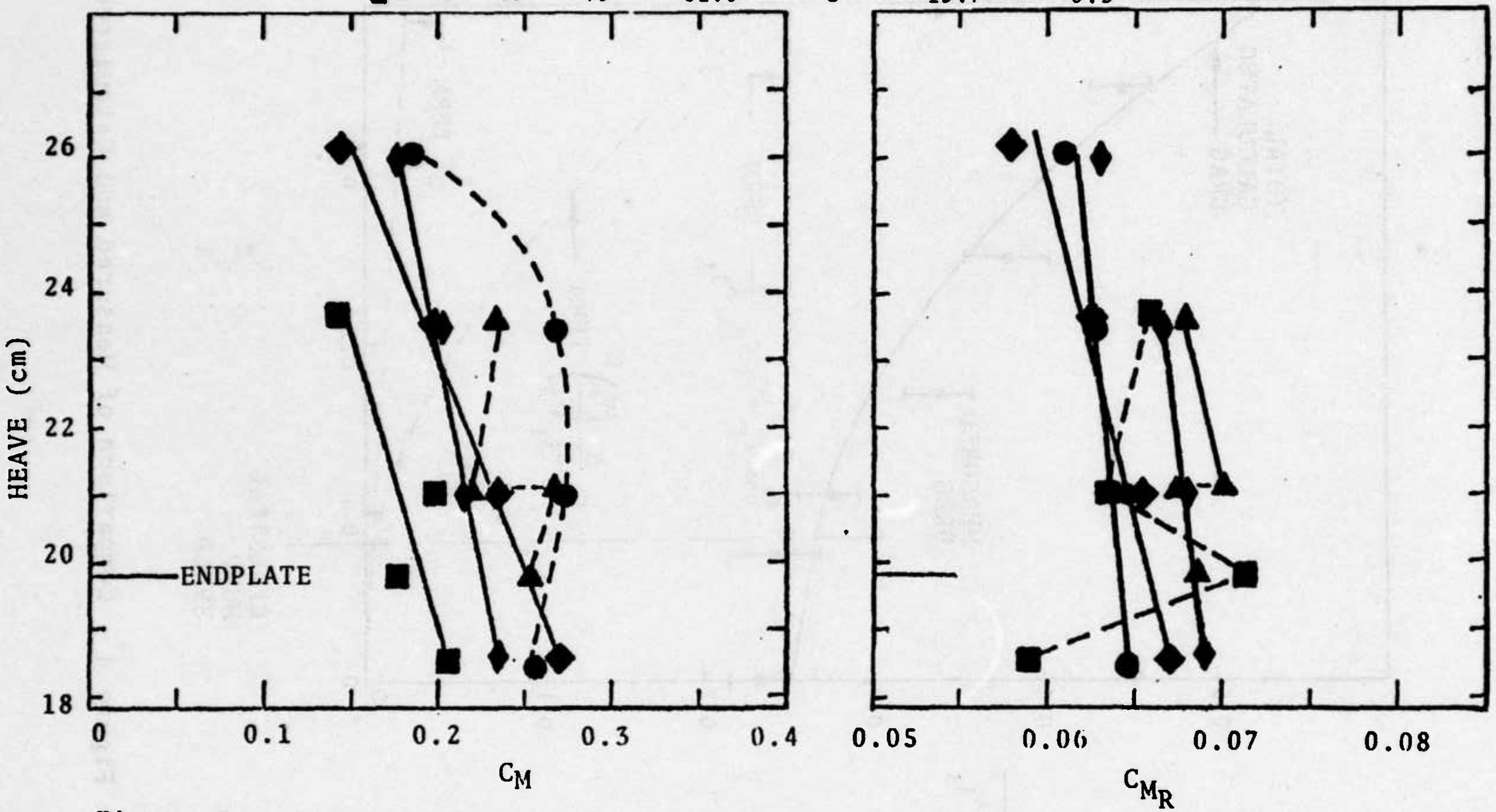

Figure 5a - Aerodynamic Moment Coefficient Figure 5b - Ram Moment Coefficient

Figure 5 - Aerodynamic and Ram Moment Coefficients versus Heave

LME